Sub-vertical low-velocity zone from P and S wave local tomography of the aftershock sequence of the Mw5.9 Chenoua (Algeria) earthquake of October 29, 1989: relict of the Miocene Eurasia–Africa suture zone?

Maya Aouad, Jérôme van Der Woerd, Catherine Dorbath, Abdallah Bounif

Sub-vertical low velocity zone from P and S waves local tomography of the aftershock sequence of the Mw5.9 Chenoua (Algeria) earthquake of 29 October 1989: relict of the Miocene Eurasia-Africa suture zone ?

Maya Aouad[1], Jérôme van der Woerd[2], Catherine Dorbath[2], Abdallah Bounif[1]

Affiliations

1 Université des sciences et de la technologie Houari-Boumédiène (USTHB), Institut des Sciences de la Terre, BP32 El Alia 16111 Bab Ezzouar, Alger, Algeria

2 Institut de Physique du Globe de Strasbourg, UMR7516, CNRS, Université de Strasbourg, 5, rue René Descartes 67000 Strasbourg, France jeromev@unistra.fr

3/10/2018

Submitted to: Journal of Seismology

Abstract

Travel-time data from the aftershock sequence following the Mw5.9 Chenoua earthquake of 29 October 1989 are inverted to obtain a 3 dimensional tomographic image of the region. The data are P and S waves travel-times obtained from 394 carefully selected aftershocks recorded at 18 temporary stations between 7 and 18 November 1989. A 3-dimensional P-wave velocity model down to a depth of 10 km is obtained. At shallow depth, the velocity contrasts clearly outline the Plio-Quaternary sedimentary basins separated by the Chenoua bedrock high. Below 4 km, a sub-vertical East-West low velocity zone can be seen down to the limit of the resolved model. The fault activated during the Chenoua event, as depicted by the aftershocks distribution is oblique to this structure and north of it. The location and geometry of the low velocity zone suggest it may correspond to a structure belonging to the suture between Eurasia and Africa, a former north dipping subduction zone, now a block boundary inherited from the Miocene collision phase. This structure may partly constrain the shallower deformation and could be responsible of the localized Sahel anticline north of the stable Mitidja basin.

Keywords: Chenoua 1989 and Tipaza 1990 earthquakes, P and S waves local tomography, seismotectonics, Eurasia-Africa collision zone

1. Introduction

Present-day seismic activity of the northern Algerian margin is a response to Plio-Quaternary NNW-SSE shortening of the Miocene Eurasia-Africa collision belt. Understanding the distribution of seismicity and the locus of large earthquakes implies to better document the active faults as well as the major structures of the crust resulting from various collision phases.

The general geodynamic evolution of the Algerian margin is dominated by the northward drift of the African continent together with subduction and oceanic accretion in the Mediterranean domain (e.g. Benaouali et al. 2006; Tapponnier 1977). After an episode of south vergent shortening in the southern Atlas during the Eocene, the north vergent Miocene subduction of the Algerian margin lead to the collision of the Maghrebides and emplacement of a stack of flysh nappes. Following slab breakoff, and opening of the Algerian oceanic Mediterranean basin (Leprêtre et al. 2013), isostatic rebound of the flexured margin led to generalized uplift along the southwestern Mediterranean coast (e.g. Pedoja et al. 2011). Presently, Africa is converging at a rate of 5-7 mm/yr towards the north (Nocquet and Calais 2004; Serpelloni et al. 2007; Figure 1 inset), reactivating the Tellian and Atlas fold and thrust belts (Benaouali et al. 2006), as well as inverting the steep previously transtensional continent-ocean Algerian margin (Strzerzynski et al. 2010; Déverchère et al. 2005; Domzig et al. 2006). North and south vergent anticlinal folding of the crustal slivers along the north-central coast of Algeria is probably responsible of most of the present-day coastal uplift, while relaxation of the margin flexure may still be responsible for part of a long wavelength uplift (Morel and Meghraoui 1996; Meghraoui et al. 1996; Pedoja et al. 2013; Authemayou et al. 2016).

The magnitude Mw5.9 Chenoua earthquake of 29 October 1989 is one of the 5 largest events that occurred in northern Algeria in the last 40 years since the 1980 El Asnam event (Figure 1; El Asnam Mw7.3 1980; Constantine Ms5.9 1985; Chenoua Mw5.9 1989; Zemmouri Mw6.8 2003; Beni Ilmane Ms5 2010; see also Table 1). Focal mechanisms of these earthquakes as well as those of smaller events indicate mostly NW-SE to NNW-SSE reverse faulting (e.g. El Asnam or Zemmouri; Delouis et al. 2004) or NE-SW left-lateral faulting on sub-vertical faults (Beni-Illmane; Yelles et al. 2013). The hypocentral depths of these earthquakes and their aftershock sequence generally remain in the mid to upper crust, i.e., above 10 km, and rarely down to 15-20 km (e.g. Zemmouri earthquake, Bounif et al. 2004). The coherent stress depicted by the seismicity and the depths of the earthquakes imply that the crust is currently undergoing shortening involving structures inherited from the previous collisional events of the Miocene in the Tell and Atlas to the south along south vergent structures, and inverted structures or new reverse faults in the north along the Mediterranean margin (e.g., Roca et al. 2004; Benaouali et al. 2006; Yelles et al. 2009).

Local tomography studies in the Maghrebides (Chiarabba et al. 1997; Bounif et al. 1998, 2004; Abacha et al. 2014; van der Woerd et al. 2014; Bellalem et al. 2015) and elsewhere (e.g.

Thurber et al. 1983; Eberhart-Philips and Michael 1993; Dorbath et al. 1996, 2008) following moderate to large earthquakes enable to highlight the upper structural levels of the crust, sedimentary basin depths and extension (Aktar et al. 2004) or décollement levels of the thrusted Miocene nappes (van der Woerd et al. 2014), major crustal faulted block boundaries (Dorbath et al. 2008; van der Woerd et al. 2014), crustal block juxtaposition in relation with seismic segmentation (Bounif et al. 1998), rupture segmentation in relation with pre-existing inverted normal faults (Chiarabba et al. 1997; Bellalem et al. 2015).

In this manuscript we use the aftershock records of the Chenoua 1989 Mw5.9 earthquake to highlight the local crustal structure using P wave travel time data of the region west of Algiers along the Chenoua and Sahel anticlines (Figures 1 and 2).

2. The Chenoua Mw5.9 earthquake of 29 October 1989

In this study we use the same dataset as in Bounif et al. (2003), namely the aftershocks recorded by 2 local networks of temporary stations deployed during 15 days 2 weeks after the main shock of 29 October 1989 (Figure 2). We will thus first summarize the main results from this and other works about the analysis of the aftershock sequence of the Chenoua earthquake.

The Chenoua earthquake occurred on 29 October 1989 at 19h:09m:12.9s (UT). It affected the region around the Chenoua massif located about 70 km to west-southwest of Algiers. It is the largest event that occurred in the Tellian Atlas after the events of El Asnam Mw6.9 of 10 October 1980 (e.g. Ouyed et al. 1981; Philip and Meghraoui 1983) and Constantine Mw5.4 of 27 October 1985 (Bounif et al. 1987; Deschamps et al. 1991) and before the Zemmouri Mw6.8 earthquake of 21 Mai 2003 (e.g. Ayadi et al. 2003, 2008; Meghraoui et al. 2004). The earthquake of maximum intensity MSK VIII (e.g. Yelles 1991) felt until Algiers caused 35 casualties and 700 injuries, affected many cities and villages and completely destroyed ancient houses mostly along the southeast flank of the Chenoua massif.

The main shock has been located by various international networks (NEIC/USGS, CSEM, ISC) and by the national network (CRAAG) (Figure 2). Because the nearest stations are far from the epicenter and because there are no close stations to the north in the Mediterranean the locations are not very robust (Figure 2). Bounif et al. (2003) have relocated the main shock using a master event method. While the location is still uncertain, they have shown that the main shock is most probably located to the south-southwest of the following better-recorded aftershock sequence (Figure 2), favoring a mainly northeastward propagation of the rupture. The depth of the main shock is not well constrained by the international and national networks. Given the depths of the aftershocks, the main shock may have been located around 10 km depth (Bounif et al. 2003).

Inversion of body waves indicates that the Chenoua earthquake mechanism is a nearly pure

reverse fault striking N66°E and dipping 56° to the NW (Bounif et al. 2003) in good agreement with the CMT Harvard centroid, which has a more northerly strike (N51E; Table 1). The main shock may be decomposed in two sub-events of 3 s and 4 s durations, respectively, with a similar mechanism and with the rupture propagating from SW at 13 km depth to the NE at 8 km depth. Both the seismic moment (8.2e17 N.m) and the size of the aftershock cloud (about 13-15 km long by 10-12 km wide) concur to the moment magnitude Mw5.9 (average slip of 20 cm; Bounif et al. 2003). Given the depth of the main shock and the slip value, surface ruptures if any would be small. A set of secondary surface slips have been reported for a length of about 4 km along the southern flank of the Chenoua massif with about up to 12 cm of vertical displacement (south up) in sub-vertical bedded Neogene conglomerates (Meghraoui 1991). The geometry and kinematics of these surface ruptures relative to the aftershock distribution (Bounif et al. 2003) suggest secondary deformation linked to the overall SW-NE anticlinal folding above a reverse fault dipping to the NW as underlined by the aftershock sequence (Bounif et al. 2003) and the overall tectonic structure deduced from offshore seismic sections (Domzig et al. 2006).

About 3 months after the Chenoua main shock, another sequence started a few kilometers to the east, northeast of Tipaza. A main shock of magnitude Ms 4.9 occurred on 9 February 1990 at 9h:30m:30s (36.78°N, 2.48°E after ISC; Figure 2). It was followed by a sequence of aftershocks that migrated towards the west-southwest and towards depth forming two distinct aftershock clouds (Figure 2; Sebaï 1997). The two northeast-southwest trending clouds are located at about 5-10 km and 10-15 km depths and extend over a length of 20 km. While the main shock is not well located, the time-evolution of the aftershock sequence suggests that the main shock is associated to the easternmost shallowest aftershocks cloud around 2.56°E 36.58°N and a depth of 7-10 km (Sebaï 1997). The overall northwest dipping aftershock clouds (Figure 2) suggest activation of a northwest dipping reverse fault as suggested by the shallow dipping fault plane of the focal mechanism of the Harvard CMT (218 123 75)(event 8 in Figure 1A and Table 1). Both aftershock clouds have been interpreted as reverse ramps linked by a flat décollement and responsible of the Sahel anticlinal growth (Maouche 2002; Harbi et al. 2004; Figure 1B).

3. Geologic and tectonic setting

The Chenoua massif, located between the cities of Cherchell and Tipaza (Figures 1 and 2), belongs to the Algerian Sahel, or more generally to the Maghrebides mountains. It forms, together with the Algiers massif, the Petite and Grande Kabylie, a set of massifs along the Mediterranean coast that belong to the internal part of the collision belt resulting from the north directed Neo-Thetys subduction during Cretaceous – lower Tertiary (Aïfa et al. 1996; Ayme et al. 1962). The suture that limits these massifs to the south is formed mostly by volcano-sedimentary units (Figure

1). Towards the Mediterranean a passive margin develops, with probably sinistral deformation during the extrusion towards southwest of the Alboran block and the opening of the Algerian-Balearic basin (e.g. Tapponnier 1977; Frizon de Lamotte et al. 2009).

The mainly NS compressive deformations from the Tertiary (EW anticlinorium and south directed reverse faulting) have exhumed in the center of the massifs pre-Cambrian metamorphic series (metamorphic unit of Brinshel), Devonian-Carboniferous series and the Mesozoic limestone series of the Kabylide. A folded Neogene sequence (continental conglomerate) together with basaltic magmatism (Belhaï 1987) follows emplacement of the Paleogene (Eo-Oligo-Miocene) flysh nappes (Belhaï et al. 1990). In addition, the mostly north-south Plio-Quaternary compression is superimposed, this time involving the reactivated passive margin to the north with mostly offshore structures (e.g. Yelles et al. 2009) .

The present-day convergence between Eurasia and Africa as determined from the plate tectonics and geodetic GPS data is oriented NW-SE and on the order of 5 mm/yr (e.g. McClusky et al. 2003; Nocquet and Calais 2004; Serpelloni et al. 2007; Figure 1, inset). This convergence of the plates at the longitude of the Chenoua massif is distributed among the Tell in the south to the alpine mountain belts of the Pyrenees and Alps to the north across the Iberian-Balearic zone. About 3 to 4 mm/yr is accommodated in northern Algeria, from the north Algerian margin across the Sahel and Tellian Atlas, to the Atlas in the south (Serpelloni et al. 2007) in agreement with the overall seismicity of this region (Figure 1).

In addition to the south vergent reverse faults and folds of the coastal mountains (Sahel, Chenoua, Thenia)(e.g. Boudiaf et al. 1998; Figure 1), north directed thrust faults affect the continental margin deforming the margin sediments (e.g. Déverchère et al. 2005; Yelles et al. 2009; Leprêtre et al. 2013). The active deformation is characterized by thrust earthquakes like the Mw6.8 Zemmouri event of Mai 2003 (Delouis et al. 2004; Bounif et al. 2004; Meghraoui et al. 2004; Déverchère et al. 2005; Semmane et al. 2005; Ayadi et al. 2008; Belabbes et al. 2009; Figure 1).

The Chenoua mountain is a 13 km-long by 8 km-wide massif with elevations reaching 905 m to the northwest of the Mitidja basin (Figures 1 and 2). The slightly east-dipping relief is truncated by a NE-SW structure to the east that make up the particular shape of the coast west of the city of Tipaza. Given mainly NS shortening during the Tertiary and the present-day strain (e.g. Nocquet 2012; inset in Figure 1), it is expected that the NE-SW striking faults are sinistral, the NW-SE faults dextral and EW faults or ENE-WSW essentially associated to folds or active thrust faults. Quaternary deformation is attested along the southern Sahel ridge in the Mitidja basin (e.g. Glangeaud 1955; Domzig et al. 2006).

4. Data and methods

The 1989 Chenoua earthquake has been followed by numerous aftershocks from which 1300 were recorded by a temporary network of 18 short period seismic stations installed between 31 October 1989 and 6 January 1990 (Figure 2; Table 2). From the 1300 records, the best-localized 394 events from November 7^{th} to 18^{th} were selected, when all the 18 stations were operational (Bounif et al. 2003). Because the main shock and most of the aftershocks are offshore, the azimuthal coverage is weak (Figure 2). Reading precision of arrival times are 0.05s for P waves and 0.1s for S waves. The selected aftershocks with magnitudes ranging from 0 to 3.1 were localized with a minimum of 9 arrivals and 2 S waves, and have a rms <0.35s with a mean of 0.18s, and horizontal and vertical mean errors of 0.84 km and 1.06 km, respectively.

Positive P wave residuals (observed minus calculated travel times) at the stations form a WSW-ENE elongated zone aligned with the average strike of the Sahel anticline and negative residuals are located along the northern flank of the Chenoua massif (Figure 3). Average residuals represent the seismic waves velocity under the stations at shallow or intermediate depths where the seismic rays are the densest. Positive residuals correspond to lower velocities as compared to the a priori model, negative ones to higher velocities. The residual mapping (Figure 3) is thus a simplified first order view of the tomographic models described below.

P and S waves travel times were used to determine the 3D structure of the velocity model under the Chenoua massif and to refine the spatial distribution of seismic hypocenters. We used the TomoDD program (Zhang and Thurber 2003), and the post-processing weighted average model (WAM) method to stabilize the velocity model (Calo et al. 2009, 2011). The double difference tomography (Zhang and Thurber 2003) combines the relocalisation method HypoDD (Waldhauser and Ellsworth 2000) and the inversion method Simul (Thurber 1983). It simultaneously calculates the 3D velocity model with a higher precision in the seismic source regions and relocates the hypocenters. TomoDD has been applied to both P and S waves. The inverted data are on one part the travel times catalog, 4823 P waves and 2693 S waves, and on the other part, the travel time differences of nearby events at the same stations. For an inter-events distance of less than 2 km, we obtain 86228 pairs of 67147 P waves and 19081 S waves. Because the number of S waves travel times are small and their readings of low quality, we present only the results from the P waves. We used the 1D velocity model of Bounif et al. (2003) to start with, with an inversion grid centered at 2.33°E and 36.583°N, and with a space between nodes of 3 km in the center, where the number of events and stations are important, and 5 km on the sides (see Appendix A1). The depth spacing is 3 km until 12 km depth, which is the maximum hypocenter depths (Bounif et al. 2003). We computed 12 tomographic inversions by changing the orientation of the grid by stepwise rotations of 15° (-15°, -30°, 45°, 60°), the position of the grid of +1km in longitude, in latitude and both together, the

depth position of -1.5km and the velocity of ±20% (Appendix A1).

The WAM method has been applied to stabilize the final velocity model (Calo 2009). This method that can be applied to all tomographic inversions is based on resampling a velocity model ensemble. The final distribution of the velocity model is a weighted mean of the resolution estimates at each node (derivative weight sum DWS parameters) calculated during tomoDD inversions. From previous inversions we built the weighted average model (WAM) by keeping only the velocity values at nodes where the DWS>100. During this process, the weighted standard deviation (WSTD) is calculated at each node of the WAM grid to check for stability and acceptability. The WSTD is determined by using the velocity distribution and the similar weighted scheme to obtain the final velocity model (Appendix A2; Calo et al. 2013a, 2013b).

5. Results

The main results obtained by the WAM carried out in the region of the Chenoua concerning velocities and relocated hypocentres are presented in figures 4 and 5. Figure 4 shows the P waves velocities for layers at 0, 3, 6 and 9 km depths, as well as the locations of hypocentres located around each levels to +/-1.5 km.

Relocated hypocentres

The 3D velocity model has been calculated with the weighting procedure of the Wam method and is used to refine the aftershock relocations. While the relocalization of the aftershocks has improved with the new velocity model of this study (Figure 2), the aftershock cloud bears nevertheless the same characteristics as those already described in Bounif et al. (2003). The aftershocks mostly depict a NE-SW striking structure (N40-50°E), about 15 km long and dipping about 55° to the northwest from 1-2 km below the surface to a depth of about 10 km (Figure 2).

Vp horizontal sections

We discuss in the following 4 horizontal sections of the model at 0, 3, 6 and 9 km depths (Figure 4). At the surface the model is only resolved in the vicinity of the stations. At 6 and 9 km, in the middle of the 3D velocity model, the tomography is best resolved. At 9 km, due to less numerous aftershocks the resolution decreases.

In the near surface model (depth of 0 km), we observe a large low velocity ($3 \leq Vp \leq 4$ km/s) NE-SW trending area and two high ($5 \leq Vp \leq 5.5$ km/s) velocity circular anomalies, one of which is located at the same place as the shallowest aftershocks. Note that the pattern of the surface layer is very similar to the picture of P wave residuals averaged at each station as shown in Figure 3.

At 3 km depth, two high velocity regions with velocities reaching 6 km/s are distinguished,

the one to the east was already observed at the surface. At this depth, the model is dominated almost entirely by low velocities 4.5≤Vp≤5 km/s, which seem to mark the extension towards depth of the slow anomalies described at the surface.

At 6 km depth the velocity pattern is changing. An EW zone of velocities about 5≤Vp≤5.5 km/s is visible in the center of the tomographic map, and higher velocities (6≤Vp≤6.5 km/s) are present north and south of it.

At 9 km depth, the pattern seen at 6 km depth is reinforced with a clear EW lower velocity anomaly right under the coastal massifs that showed higher velocities near the surface.

Vp vertical sections

In Figures 5A and 5B are presented 10 Vp vertical sections projected N135 and NS, respectively (see location of sections in Figure 4). The N135 projection is perpendicular to the present-day active structures and the seismicity trend of the 1989 aftershocks, while the NS projection is perpendicular to the main tomographic anomaly at depth (slices 6 and 9 km, figure 4). Relocated hypocentres in the vicinity of the section are also projected.

The sections highlight the patterns already described above for the tomographic slices (Figure 4). The sections show clearly the low velocity anomalies of the surface down to a few kilometers separated by the localized high velocity anomalies that extend to larger depth (sections 4 and 6 in figure 5A). Below 5 km, the pattern of anomalies is changing with a low velocity anomaly appearing below the high velocities of the surface. The NS sections clearly show that this low velocity anomaly is striking EW and extends to depths of 10 km.

6. Discussion

6. 1 Previous tomographic studies in the Algerian Tell

The first tomographic study in Algeria has been performed by Chiarabba et al. (1997) using the aftershocks sequence of the El Asnam earthquake (October 10, 1980, Ms7.3)(Figure 1). Following the usual interpretation that velocity anomalies in the shallow crust are closely linked to lithologic heterogeneities (e.g. Eberhart-Phillips and Michael 1993; Foxall et al. 1993; Chiarabba et al. 1995), the high velocities observed in the footwall of the fault have been related to the presence of pre-Neogene basement. Another rapid anomaly has been linked to Mesozoic limestone formations along a former normal fault along the pre-Neogene basement, and a low velocity anomaly region corresponds to the quaternary sedimentary deposits of the Chelif basin. A more recent tomographic study (Bellalem et al. 2015) in the same region using more data and a new code corroborates the former results.

The Constantine earthquake (October 27, 1985, Ms5.9) aftershocks sequence was used to compute a 3D velocity model of the P wave to a depth of 12 km (Bounif et al. 1998). The near surface low velocities (3.5 km/s) were associated to Mio-Pliocene and Quaternary deposits, while the high velocities (5.5 km/s) were related to the Constantine neritic and the Tellian Jurassic to Paleogene calcareous nappes. The depth extension of the velocity contrasts constrains the few kilometers nappes thickness.

Following the Zemmouri earthquake (May 21, 2003, Mw6.8) the 3D P wave velocity model based on the aftershocks sequence travel times (Ayadi et al. 2008), not only confirmed the upper layer distribution of Quaternary deposits and marine terraces (low velocities 4.5 to 5 km/s) and basement outcrops (high velocities) but highlighted a clear structural contact between the Blida thrust and fold belt (low velocities) and the metamorphic Kabylie basement block (high velocities). The more recent tomographic inversion (Kherroubi et al. 2017) based on the LOTOS program and a denser database confirmed previous results.

A more recent tomography in the region of the shallow Beni Ilmane earthquake of May 14, 2010 of moderate magnitude (Md5.2) and its aftershock sequence mostly constrained the upper crustal (< 6 km) geological units and major geological structures (Abacha et al. 2014; Baldini 1966).

In general, aftershocks sequence tomographies from moderate to large earthquakes in slow deforming regions show no link between the distribution of seismicity and the 3D velocity pattern. The models tend to confirm the first order surface geology, in particular the major geological structures such as sedimentary basin regions (low velocities) and basement zones (high velocities). Major structural boundaries may be depicted at depth when the resolution is high enough, usually associated to the presence of deep seismic events (e.g. Zemmouri earthquake; Ayadi et al. 2008).

6.2 3D velocity model in the Chenoua region

Near the surface and down to a few kilometers the contrasts correspond very well to the surface geology (Figures 4 and 5). The low velocities around 3 km/s are related to the Tertiary to Quaternary sediments of the Mitidja basin and surrounding piedmonts of the Tellian Atlas to the south. Low velocities are also seen north of the Chenoua massif related to coastal sediments although the resolution becomes weaker in the absence of stations to the north. As discussed above and observed on other tomography models, the seismicity recorded for the Chenoua sequence seems to be distributed randomly among fast and low velocity zones (Figures 4, 5A and 5B), which characterizes mostly slow deforming zones where earthquakes are of moderate size, have very large recurrence times, and not very large cumulative displacements. In this case, the seismic activity is not strong enough to modify significantly the rheological properties of the crust. The only structural

315 link observed is the seismicity alignment with the overall topography of the Chenoua massif and
316 thus the surface geology. Active folding is uplifting the Chenoua massif with its Palaeozoic
317 metamorphic core covered by Tertiary sediments above a NE-SW striking NW dipping thrust fault
318 (Figures 1 and 2).
319 Deeper, the present-day seismicity seems even more disconnected from the structures visible
320 in the tomography (Figures 4C and 4D). An E-W striking low velocity zone is observed at 6 km,
321 and even better at 9 km. Because there is no link with the present-day active deformation, the
322 presence of an E-W striking low velocity zone has to be linked with inherited structures from
323 former tectonic events. This sub-vertical E-W striking low velocity zone at the base of the upper
324 crust is thus most certainly linked to the N-S convergence during the Miocene subduction of the
325 Algerian margin. Whether this low velocity zone corresponds to subducted low-density upper
326 crustal rocks or sediments, or to a fluid rich shear zone of the former subduction cannot be
327 determined. Its position and geometry suggest it belongs to the structures emplaced during the
328 Miocene suturing event (Figure 1B).
329 The structures evidenced by the local tomography, together with the present-day thrust
330 geometry as evidenced by the aftershock sequences of the 1989 and 1990 events near Tipaza, thus
331 depict the collision zone of the north Algerian coastal margin (Figure 1B). Two domains are
332 outlined. The first domain to the north, with a complex structure of NE-SW oblique reactivated
333 faults (Chenoua, Tipaza and Alger anticlines), north of a more simple and probably younger and
334 shallower more linear fault (the Sahel anticline) (Figure 1D). These thrusts are south verging but
335 remain north and do not cross-cut the domain boundary. The second domain comprises the Mitidja
336 basin, which remains largely undeformed, but flexured by overthrusting of the Algerian margin. We
337 thus suggest that the geometry of the main structures presently active along the coast near Algiers
338 reflects the structuration of the margin during the Miocene collision. However, because present-day
339 convergence is ongoing and oriented NW-SE (Figure 1, inset), obliquely to the more N-S oriented
340 Miocene convergence (e.g. Benaouali et al. 2006), shortening extends at the front of the Algerian
341 margin along SW-NE striking structures (Figure 1), such as the the Khair-al-Din thrust fault or the
342 set of Boumerdès thrust faults more to the east (e.g. Yelles et al. 2009; Déverchère et al. 2005).
343
344 **7. Conclusion**
345 Reconstructing the structuration of the lithosphere can help understanding the present-day
346 pattern of deformation. Local seismic tomography gives the opportunity to illuminate structures
347 down to the middle crust. In this study we show the presence of a major velocity anomaly down to a
348 depth of 10 km probably linked to the Miocene subduction along the Algerian margin. This
349 structure possibly associated to the suture of Eurasia and the African plate is presently the locus of

localized strain as depicted by recent large earthquakes such as the Chenoua Mw6 event of 1989 and active folding in the Sahel ridge.

Acknowledgments

We thank Louis Dorbath for fruitfull discussions and comments during manuscript preparation. Marco Calo is thanked for sharing its expertise with the WAM model computing and outputs. Nathalie van der Woerd helped for the various plots used in the figures. Maya Aouad is thankfull to the USTHB for supporting her travel and visits to Strasbourg at EOST and IPGS in the frame of her PhD.

References

Abacha I, Koulakov I, Semmane F, Yelles-Chaouche A (2014) Seismic tomography of the area of the 2010 Beni-Ilmane earthquake sequence, north-central Algeria. SpringerPlus 3:650. doi: 10.1186/2193-1801-3-650

Aïfa T, Belhaï D, Merle O (1996) Paléopôle dévonien pour le massif du Chenoua (Algérie): accrétion du domaine Kabyle à l'Afrique. C R Acad Sci 322(IIa):685-691

Aktar M, Dorbath C, Arpat E (2004) The seismic velocity and fault structure of the Erzincan Basin, Turkey, using local earthquake tomography. Geophys J Int 156 :497-505

Authemayou C, Pedoja K, Heddar A, Molliex S, Boudiaf A, Ghaleb B, Van Vliet Lanoe B, Delcaillau B, Djellit H, Yelles K, Nexer M (2016) Coastal uplift west of Algiers (Algeria): pre- and post-Messinian sequences of marine terraces and rasas and their associated drainage pattern. Int J Earth Sci (Geol Rundsch). doi: 10.1007/s00531-016-1292-5

Ayadi A, Maouche S, Harbi A et al (2003) Strong Algerian earthquake strikes near capital city. Eos Trans AGU 84(50):561-568

Ayadi A, Dorbath C, Ousadou F, Maouche S, Chikh M, Bounif MA, Meghraoui M (2008) Zemmouri earthquake rupture zone (Mw 6.8, Algeria): aftershocks sequence relocation and 3D velocity model. J Geophys Res 113(B09301). doi: 10.1029/2007JB005257

Ayme A, Ayme JM, Bouillin M et al (1962) Carte géologique de l'Algérie 1:50 000, 40 Tipaza. Service de la carte Géologique de l'Algérie, Alger

Baldini P (1966) Notice explicative de la carte géologique au 1/50 000 « TARMOUNT » Feuille 140. Service géologique de l'Algérie, Alger.

Belabbes S, Wicks C, Cakir Z, Meghraoui M (2009) Rupture parameters of the 2003 Zemmouri (Mw6.8), Algeria, earthquake from joint inversion of interferometric synthetic aperture radar, coastal uplift, and GPS. J Geophys Res 114(B03406). doi: 10.1029/2008JB005912

385 Belhaï D (1987) Massif du Chenoua (Algérie) : mise en place des flysches en relation avec un
386 cisaillement “transcurent” E-W, responsable de la structure en éventail. Mémoire de
387 magister, Université des Sciences et de la Technologie Houari Boumediene (USTHB),
388 Alger, Algerie
389 Belhaï D, Merle O, Saadelah A (1990) Transpression dextre à l'Eocene supérieur dans la chaîne des
390 Maghrébides (massif du Chenoua, Algérie). C R Acad Sci Paris 310(II):795-800
391 Bellalem F, Bounif MA, Koulakov I (2015) P and S waves tomographic analysis of the area of El
392 Asnam’s 1980 Ms 7.3 earthquake (Algeria) from its aftershock sequence. J Seismol. doi:
393 10.1007/s10950-014-9464-x
394 Benaouali N, Frizon de Lamotte D, Roca E, Bracene R, Faure JL, Sassi W, Roure F (2006) Post-
395 Cretaceous kinematics of the Atlas and Tell systems in central Algeria: early foreland
396 folding and subduction-related deformation. C R Geoscience 338:115-125.
397 doi:10.1016/j.crte.2005.11.005
398 Boudiaf A, Ritz JF, Philip H (1998) Drainage diversions as evidence of propagating active faults:
399 example of the El Asnam and Thenia faults, Algeria. Terra Nova 10(5):236-244
400 Bounif MA, Haessler H, Meghraoui M (1987) The Constantine (northeast Algeria) earthquake of
401 October 27, 1985: surface ruptures and aftershock study. Earth and Planetary Sci Lett
402 85(4):451-460
403 Bounif MA, Dorbath C (1998) Three dimensional velocity structure and relocated aftershocks for
404 the 1985 Constantine, Algeria (Ms=5.9) earthquake. Annali di Geofisica 41(1) :93-104
405 Bounif MA, Bezzeghoud M, Dorbath L, Legrand D, Deschamps A, Rivera L, Benhallou H (2003)
406 Seismic source study of the 1989, October 29, Chenoua (Algeria) earthquake from
407 aftershocks, broad-band and strong ground motion records. Annals of Geophysics 46(4):
408 625-646
409 Bounif MA, Dorbath C, Ayadi A, Meghraoui M, Beldjoudi H, Laouami N, Frogneux M, Slimani A,
410 Alasset PJ, Kharroubi A, Ousadou F, Chikh M, Harbi A, Larbes S, Maouche S (2004) The
411 21 May, 2003 Zemmouri (Algeria) earthquake Mw 6.8: Relocation and aftershock sequence
412 analysis. Geophys Res Lett 31(L19606). doi: 10.1029/2004GL020586
413 Calo M (2009) Tomography of subduction zones using regional earthquakes: methodological
414 developments and application to the Ionian slab. PhD thesis, Université de Strasbourg, pp1-
415 134. http://tel.archives-ouvertes.fr/tel-00438598/en/
416 Calo M, Dorbath C, Luzio D, Rotolo S, D'anna G (2009) Local earthquake tomography in the
417 southern Tyrrhenian region of Italy: Geophysical and petrological inferences on the
418 subducting lithosphere. Subduction Zone Geodynamics. Frontiers in Earth Sciences 85–99
419 eds Lallemand S & Funiciello F, Springer-Verlag, Berlin, Heidelberg. doi:10.1007/978-3-

540-87974-9

Calo M, Dorbath C, Cornet FH, Cuenot N (2011) Large-scale aseismic motion identified through 4-D P-wave tomography. Geophys J Int 186(3):1295-1314. doi: 10.1111/j.1365-246X.2011.05108.x

Calo M, Dorbath C (2013a) Different behaviours of the seismic velocity field at Soultz-sous-Forêts revealed by 4D seismic tomography: case study of GPK3 and GPK2 injection tests. Geophys J Int 194:1119-1137. doi:10.1093/gji/ggt153

Calo M, Parisi L, Luzio D (2013b) Lithospheric P- and S-wave velocity models of the Sicilian area using WAM tomography procedure and assessments. Geophys J Int 195:625–649. doi: 10.1093/gji/ggt252

Chiarabba C, Amato A, Fiordelisi A (1995) Upper crustal tomographic images of the Amiata-Vulsini geothermal region, central Italy. J Geophys Res 100:4053-4066

Chiarabba C, Amato A, Meghraoui M (1997) Tomography images of the El Asnam fault zone and the evolution of a seismogenic thrust-related fold. J Geophys Res 102(B11):485-498

Delouis B, Vallee M, Meghraoui M, Calais E, Maouche S, Lammali K, Mahsas A, Briole P, Benhamouda F, Yelles K (2004) Slip distribution of the 2003 Boumerdes-Zemmouri earthquake, Algeria, from teleseismic, GPS, and coastal uplift data. Geophys Res Lett 31(L18607). doi:10.1029/2004GL020687

DeMets C, Gordon RG, Argus DF, Stein S (1994) Effect of recent revisions to the geomagnetic reversal time scale on estimates of current plate motions. Geophys Res Lett 21 :2191-2194

Deschamps A, Gaudemer Y, Cisternas A (1982) The El Asnam, Algeria, earthquake of 10 October 1980: multiple-source mechanism determined from long-period records. Bull Seismol Soc Am 72(4):1111-1128

Deschamps A, Bezzeghoud M, Bounif MA (1991) Seismological study of the Constantine (Algeria) earthquake (27 October 1985). Instituto Geografico National 8:163-173

Déverchère J, Yelles K, Domzig A, Mercier de Lépinay B, Bouillin JP, Gaullier V, Bracène R., Calais E, Savoye B, Kherroubi A, Le Roy P, Pauc H, Dan G (2005) Active thrust faulting offshore Boumerdes, Algeria, and its relations to the 2003 Mw 6.9 earthquake. Geophys Res Lett 32(L04311). doi:10.1029/2004GL021646

Domzig A (2006) Déformation active et récente, et structuration tectono-sédimentaire de la marge sous-marine algérienne. PhD thesis. University of Bretagne Occidentale, Brest, pp343

Domzig A, Yelles K, Le Roy C, Déverchère J, Bouillin JP, Bracène R, Mercier de Lépinay B, Le Roy P, Calais E, Kherroubi A, Gaullier V, Savoye B, Pauc H (2006) Searching for the Africa-Eurasia Miocene boundary offshore Western Algeria (Maradja'03 cruise). C R Geoscience 338:80-91. doi:10.1016/j.crte.2005.11.009

455 Dorbath, C, Oppenheimer D, Amelung F, King G (1996) Seismic tomography and deformation
456 modeling of the junction of the San Andreas and Calaveras faults. J Geophys Res
457 101(B12):27917–27941
458 Dorbath C, Gerbault M, Carlier G, Guiraud M (2008) Double seismic zone of the Nazca plate in
459 northern Chile: High-resolution velocity structure, petrological implications, and
460 thermomechanicl modeling. Geochemistry Geophysics Geosystems 9(7):1-29. doi:
461 10.1029/2008GC002020
462 Eberhart-Phillips D, Michael AJ (1993) Three-dimensional velocity structure, seismicity, and fault
463 structure in the Parkfield region, central California. J Geophys Res 98(B9):15737-15758
464 Frizon de Lamotte D, Leturmy P, Missenard Y, Khomsi S, Ruiz G, Saddiqi O, Guillocheau F,
465 Michard A (2009) Mesozoic and Cenozoic vertical movements in the Atlas system (Algeria,
466 Morocco, Tunisia): An overview. Tectonophysics 475(1):9-28. doi:
467 10.1016/j.tecto.2008.10.024
468 Foxall W, Michelini A, McEvilly TV (1993) Earthquake travel time tomography of the southern
469 Santa Cruz Mountains: Control of fault heterogeneity of the San Andreas fault zone. J
470 Geophys Res 98(B10):17691-17710
471 Glangeaud L (1955) Les deformations plio-quaternaires de l'Afrique du Nord. Inter J of Earth
472 Sciences. Geologische Rundschau 43(1):181-196
473 Harbi A, Maouche S, Ayadi A, Benouar D, Panza GF, Benhallou H (2004) Seismicity and tectonics
474 structures in the site of Algiers and its surroundings: A step towards microzonation. Pure
475 Appl Geophys 161:949-967. doi: 10.1007/s00024-003-2502-1
476 Kherroubi A, Yelles AC, Koulakov I, Déverchère J, Beldjoudi H, Haned A, Semmane F, Aidi C
477 (2017) Full aftershock sequence of the Mw 6.9 2003 Boumerdes earthquake, Algeria:
478 Space-time distribution, local tomography and seismotectonic implications. Pure Appl
479 Geophys 174:2495-2521. doi:10.1007/s00024-017-1571-5
480 Leprêtre A, Klingelhoefer F, Graindorge D, Schnurle P, Beslier MO, Yelles K, Déverchère J,
481 Bracene R (2013) Multiphased tectonic evolution of the central Algerian margin from
482 combined wide-angle and reflection seismic data off Tipaza, Algeria. J Geophys Res
483 118:3899-3916. doi :10.1002/jgrb.50318
484 Ouyed M, Meghraoui M, Cisternas A, Descamps A, Dorel J, Frechet J, Gaulon R, Hatzfeld D,
485 Philip H (1981) Seismotectonics of the El Asnam earthquake. Nature 292:26-31
486 Maouche S (2002) Etude sismotectonique de l'Algérois et des zones limitrophes de Cherchell –
487 Gouraya. Mémoire de magister, Université des sciences et de la technologie Houari
488 Boumediene (USTHB), Alger
489 McClusky S, Reilinger R, Mahmoud S, Ben Sari D, Tealeb A (2003) GPS constraints on Africa

(Nubia) and Arabia plate motions. Geophys J Int 155: 126–138

Meghraoui M (1991) Blind reverse faulting system associated with the Mont Chenoua-Tipaza earthquake of 29 October 1989 (north-central Algeria). Terra Nova 3:84-93

Meghraoui M, Morel JL, Andrieux J, Dahmani M (1996) Tectonique plio-quaternaire de la chaîne tello-rifaine et de la mer d'Alboran. Une zone complexe de convergence continent–continent. Bull Soc Géol France 167(1):141–157

Meghraoui M, Maouche S, Chemaa B, Cakir Z, Aoudia A, Harbi A, Alasset PJ, Ayadi A, Bouhaded Y, Benhamouda F (2004) Coastal uplift and thrust faulting associated with the Mw=6.8 Zemmouri (Algeria) earthquake of 21 May, 2003. Geophys Res lett 31(L19605). doi: 0.1029/2004GL020466

Morel JL, Meghraoui M (1996) Goringe-Alboran-Tell tectonic zone: a transpression system along the Africa-Eurasia plate boundary. Geology 24(8):755–758

Nocquet JM (2012) Present-day kinematics of the Mediterranean: A comprehensive overview of the GPS results. Tectonophysics 579:220-242. doi: 10.1016/j.tecto.2012.03.037

Nocquet JM, Calais E (2004) Geodetic measurements of crustal deformation in the Western Mediterranean and Europe. Pure Appl Geophys 161. doi: 10.1007/s00024-003-2468-z

Pedoja K, Husson L, Regard V, Cobbold PR, Ostanciaux E, Johnson ME, Kershaw S, Saillard M, Martinod J, Furgerot L, Weill P, Delcaillau B (2011) Relative sea-level fall since the last interglacial stage: Are coasts uplifting worldwide ? Earth Sci Rev 108:1–15. doi: 10.1016/j.earscirev.2011.05.002

Pedoja K, Djellit H, Authemayou C, Déverchère J, Strzerzynski P, Heddar A, Nexer M, Boudiaf A (2013) Comment on: "Active coastal thrusting and folding, and uplift rate of the Sahel anticline and Zemmouri earthquake area (Tell Atlas, Algeria)" by Maouche et al. Tectonophysics 601. doi: 10.1016/j.tecto.2012.08.043

Philip H, Meghraoui M (1983) Structural analysis and interpretation of the surface deformations of the El Asnam earthquake of October 10, 1980. Tectonics 2(1):17–49

Ratzov G, Cattaneo A, Babonneau N, Déverchère J, Yelles K, Bracene R, Courboulex F (2015) Holocene turbidites record earthquake supercyles at a slow-rate plate boundary. Geology 43(4):331-334.doi:10.1130/G36170.1

Roca R, Frizon de Lamotte A, Mauffret A, Bracène R, Vergès J, Benaouali N, Fernandez M, Munoz JA, Zayen H (2004) The Mediterranean region from crust to mantle. Eds by Cavazza W, Roure F, Spakman W, Stampfli GM, Ziegler PA. Springer, Berlin Heidelberg

Sebaï A (1997) Analyse sismologique des séismes récents du Sahel d'Alger. Mémoire de magister. Université des Sciences et de la Technologie Houari Boumediene (U.S.T.H.B.) Alger, pp178

Semmane F, Campillo M, Cotton F (2005) Fault location and source process of the Boumerdes,

525 Algeria, earthquake inferred from geodetic and strong motion data. Geophys Res Lett
526 32(L01305). doi:10.1029/2004GL021268
527 Serpelloni E, Vannucci G, Pondrelli S, Argnani A, Casula G, Anzidei M, Baldi P, Gasperini P
528 (2007) Kinematics of the western Africa-Eurasia plate boundary from focal mechanism and
529 GPS data. Gephys J Int 169:1180-1200. doi: 10.1111/j.1365-246X.2007.03367.x
530 Strzerzynski P, Déverchère J, Cattaneo A, Domzig A, Yelles K (2010) Tectonic inheritance and
531 Pliocene-Pleistocene inversion of the Algerian margin around Algiers: Insights from
532 multibeam and seismic reflection data. Tectonics 29(TC2008). doi: 10.1029/2009TC002547
533 Tapponnier P (1977) Evolution tectonique du système alpin en Mediterranée : poinçonnement et
534 écrasement rigide-plastique. Bull Soc Geol Fr XIX(3):437–460
535 Thurber CH (1983) Earthquake locations and three-dimensional crustal structure in the Coyote Lake
536 area, Central California. J Geophys Res 88(B10):8226-8236
537 Van der Woerd J, Dorbath C, Ousadou F, Dorbath L, Delouis B, Jacques E, Tapponnier P, Hahou
538 Y, Menzhi M, Frogneux M, Haessler H (2014) The Al Hoceima Mw 6.4 earthquake of 24
539 February 2004 and its aftershocks sequence. Journal of Geodynamics 77:89-109. doi:
540 10.1016/j.jog.2013.12.004
541 Waldhauser F, Ellsworth WL (2000) A double-difference earthquake location algorithm: method
542 and application to the northern Hayward Fault, California. Bull Seismol Soc Am 90(6):
543 1353–1368
544 Yelles A (1991) Coastal Algerian earthquakes: A potential risk of tsunamis in Western
545 Mediterranean, preliminary investigation. Science of Tsunami Hazards 9(1): 47-54
546 Yelles A, Domzig A, Déverchère J, Bracene R, Mercier de Lepinay B, Strzerzynski P, Bertrand G,
547 Boudiaf A, Winter T, Kherroubi A, Le Roy P, Djellit H (2009) Plio-Quaternary reactivation
548 of the Neogene margin off NW Algiers, Algeria: the Khayr al Din bank. Tectonophysics
549 475:98-116. doi: 10.1016/j.tecto.2008.11.030
550 Yelles A, Abacha I, Semmane F, Beldjoudi H, Djellit H (2013) The Beni-Ilmane (north-central
551 Algeria) earthquake sequence of May 2010. Pure and Applied Geophysics. doi:
552 10.1007/s00024-013-0709-3
553 Zhang H, Thurber CH (2003) Double-difference tomography: The method and its application to the
554 Hayward fault, California. Bull Seism Soc Am 93(5):1875-1889
555
556
557
558
559

560 **Figure captions**

561 **Figure 1.** A) Seismotectonic map of northern Algeria (modified from Yelles et al. 2009). Major
562 earthquakes (Mw>5) are represented together with their focal mechanisms. Bathymetry from
563 Domzig (2006). White line is position of section in Figure 1B. Inset is position of map in Eurasia-
564 Africa plate tectonic frame, vectors are relative motion between Eurasia and Africa from GPS
565 geodesy (red arrows) and plate reconstructions Nuvel-1A (white arrows, Demets et al. 1994), after
566 Serpelloni et al. (2007). PK: Petite Kabylie; C: Constantine; B: Beni Ilmane; AM: Algiers massif.
567 Dashed purple line is position of Tertiary suture.
568 B) Synthetic lithospheric scale sections perpendicular to main structures of the margin near
569 Chenoua massif. Yellow star, inferred position of Chenoua 1989 earthquake hypocenter; black dots
570 projection of aftershock clouds of Mw5.9 1989 and M5 1990 seismic sequences (see text for
571 details).
572
573 **Figure 2.** A) Aftershocks of the 29 October 1989 Mw5.9 Chenoua earthquake (circles) registered
574 by 2 local networks between 7 and 18 November 1989 (Bounif et al. 2003) and of 9 February 1990
575 Tipaza M5 earthquake (squares) (Sebaï 1997). Seismic station details in Bounif et al. (2003); B-C-
576 D-E) N135E sections across aftershock clouds from SW to NE (scale as in figure 2A).
577
578 **Figure 3.** Positive and negative P wave residuals averaged at each station. At first order, shallow
579 crustal low and fast velocity zones are depicted (see text).
580
581 **Figure 4**. P wave model slices at depths of 0, 3, 6 and 9 km. White circles are seismicity of each 3
582 km-thick slice. Line numbers (1 to 10) refer to N135 and NS sections of figures 5A and 5B,
583 respectively. Seismic stations and coastline are indicated.
584
585 **Figure 5.** A) and B) are N135 and NS sections, respectively, of the P wave model (see location in
586 figure 5). Seismicity (red circles) in the vicinity of the sections as well as nearby seismic stations
587 are also shown.
588
589 **Table 1.** Characteristics of major instrumental earthquakes shown in Figure 1.
590
591 **Appendix**
592 A1. WAM grids
593 A2. Resolution of the velocity model
594

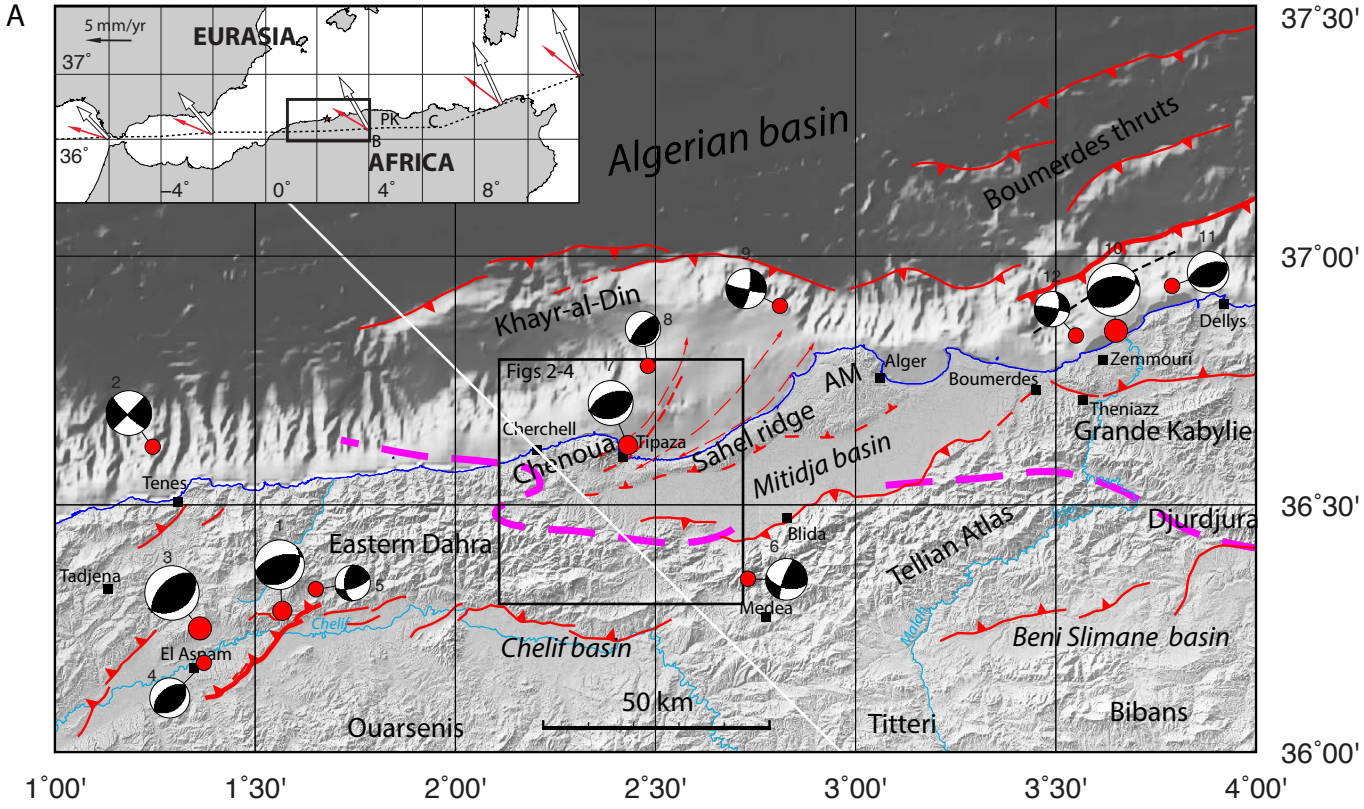
A
5 mm/yr
EURASIA
AFRICA
PK
B
C
37°
36°
−4°
0°
4°
8°
Algerian basin
Boumerdes thruts
Khayr-al-Din
Figs 2-4
Cherchell
Tipaza
Chenoua
Sahel ridge
AM
Alger
Boumerdes
Zemmouri
Dellys
Theniazz
Grande Kabylie
Mitidja basin
Djurdjura
Tellian Atlas
Tenes
Tadjena
El Asnam
Eastern Dahra
Chelif
Chelif basin
Blida
Medea
Beni Slimane basin
Titteri
Bibans
Ouarsenis
50 km
37°30'
37°00'
36°30'
36°00'
1°00'
1°30'
2°00'
2°30'
3°00'
3°30'
4°00'

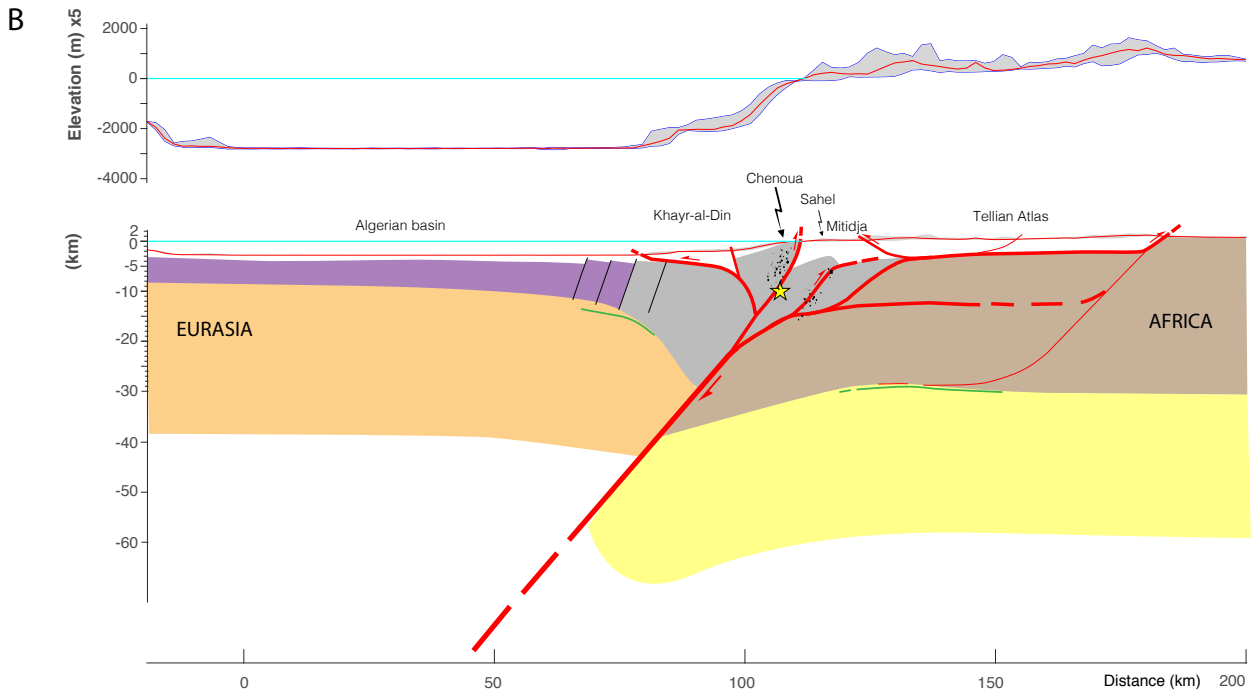
B
Elevation (m) x5
2000
0
-2000
-4000
Chenoua
Sahel
Khayr-al-Din
Mitidja
Tellian Atlas
Algerian basin
(km)
2
0
-5
-10
-20
-30
-40
-50
-60
EURASIA
AFRICA
0
50
100
150
Distance (km)
200

Figure 1

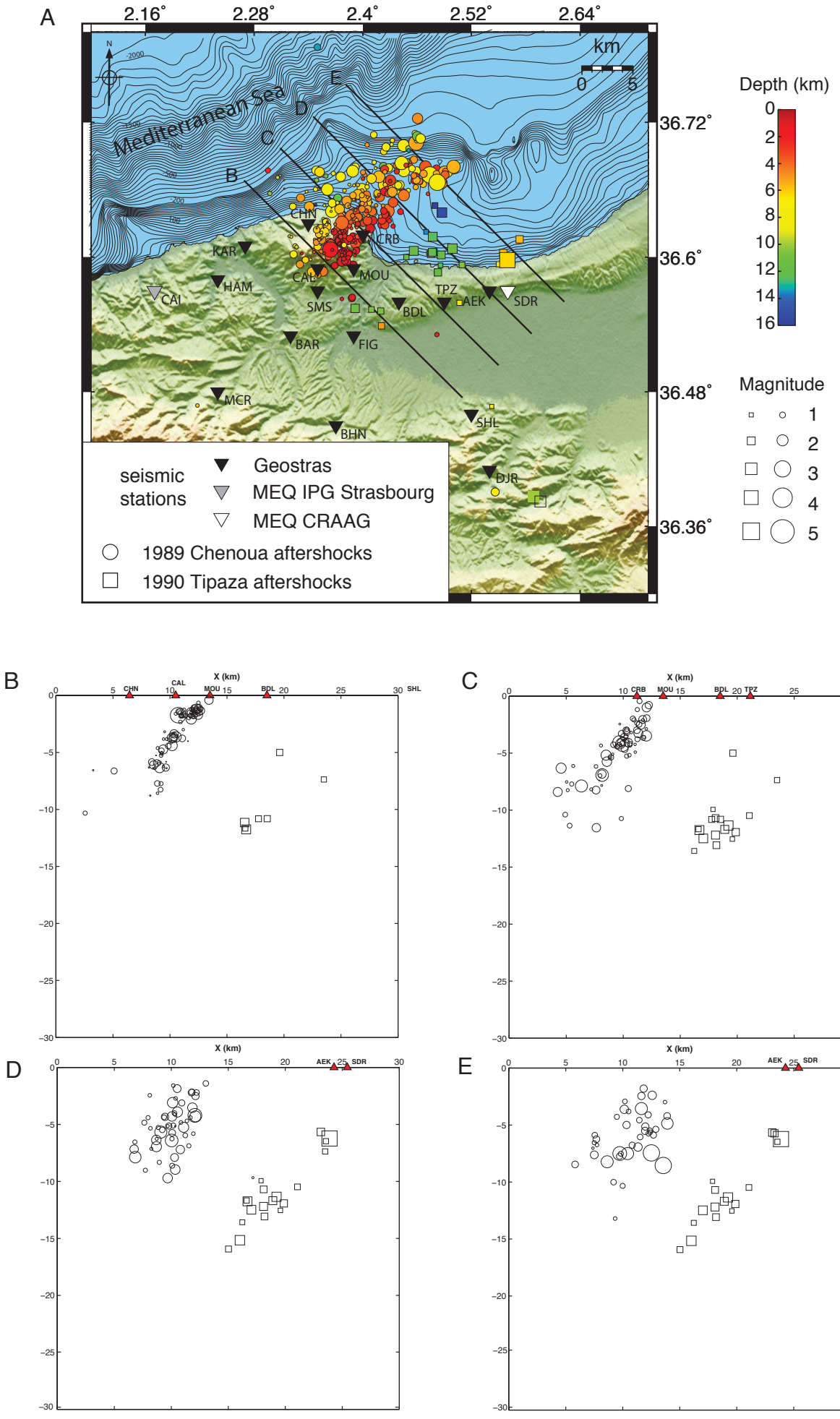
A
2.16˚
2.28˚
2.4˚
2.52˚
2.64˚
km
0
5
36.72˚
36.6˚
36.48˚
36.36˚
Mediterranean Sea
B
C
D
E
CHN
CRB
KAR
CAL
MOU
HAM
CAI
SMS
BDL
TPZ
AEK
SDR
BAR
FIG
MCR
SHL
BHN
DJR
Depth (km)
0
2
4
6
8
10
12
14
16
Magnitude
1
2
3
4
5
seismic stations
Geostras
MEQ IPG Strasbourg
MEQ CRAAG
1989 Chenoua aftershocks
1990 Tipaza aftershocks
B
C
D
E
X (km)

Figure 2

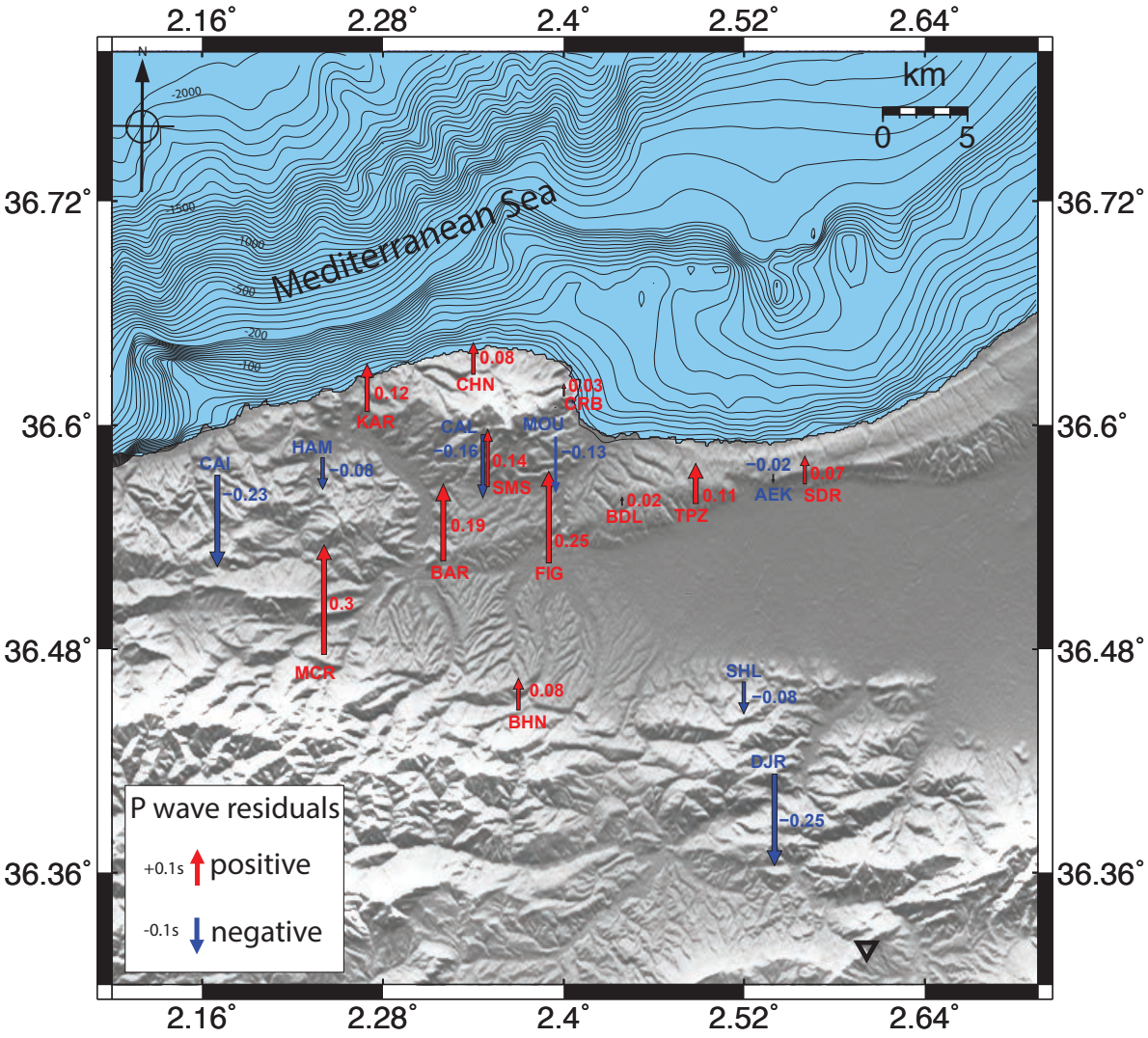
2.16°
2.28°
2.4°
2.52°
2.64°
36.72°
36.6°
36.48°
36.36°
N
km
0
5
-2000
-1500
-1000
-500
-200
-100
Mediterranean Sea
0.08
CHN
0.12
KAR
0.03
CRB
CAL
−0.16
0.14
SMS
MOU
−0.13
HAM
−0.08
CAI
−0.23
0.19
BAR
0.25
FIG
0.02
BDL
0.11
TPZ
−0.02
AEK
0.07
SDR
0.3
MCR
0.08
BHN
SHL
−0.08
DJR
−0.25
P wave residuals
+0.1s positive
-0.1s negative

Figure 3

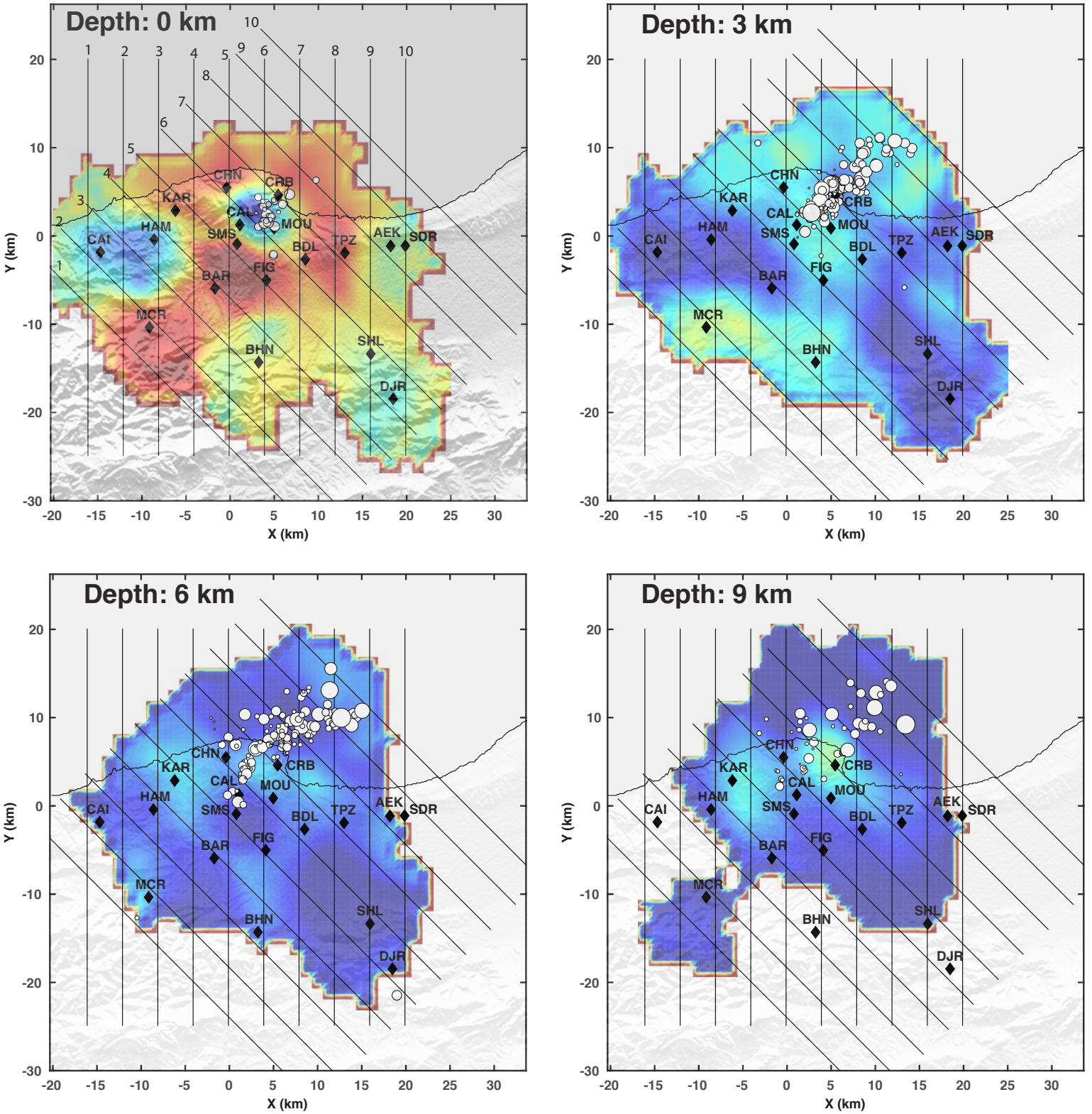
Depth: 0 km
Depth: 3 km
Depth: 6 km
Depth: 9 km
CHN
CRB
KAR
CAL
MOU
HAM
SMS
BDL
TPZ
AEK
SDR
CAI
FIG
BAR
MCR
BHN
SHL
DJR
X (km)
Y (km)
3
3.5
4
4.5
5
5.5
6
Vp (km/s)

Figure 4

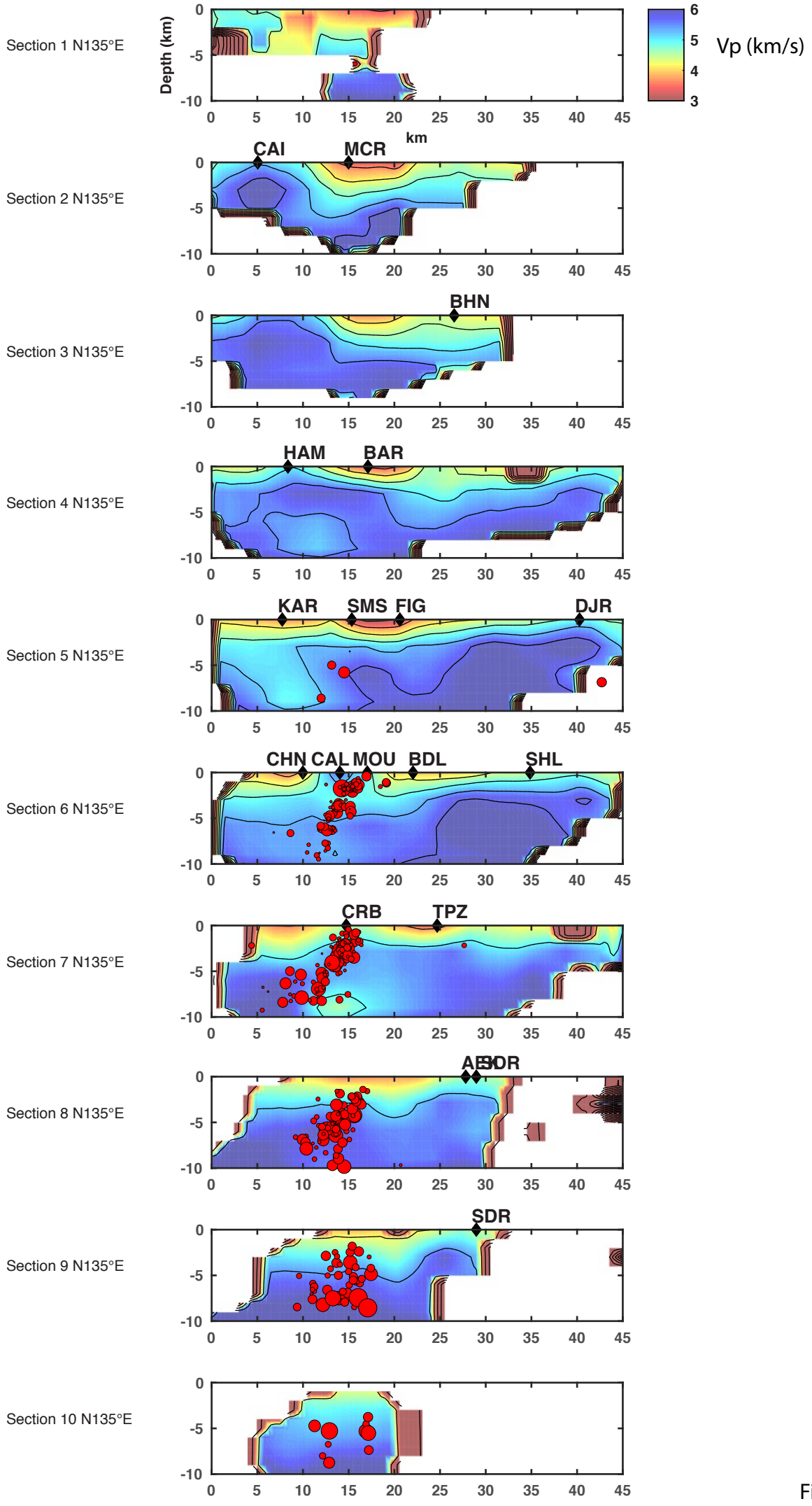
Section 1 N135°E
Depth (km)
0
-5
-10
0 5 10 15 20 25 30 35 40 45
km
6
5
4
3
Vp (km/s)
Section 2 N135°E
CAI
MCR
Section 3 N135°E
BHN
Section 4 N135°E
HAM
BAR
Section 5 N135°E
KAR
SMS
FIG
DJR
Section 6 N135°E
CHN
CAL
MOU
BDL
SHL
Section 7 N135°E
CRB
TPZ
Section 8 N135°E
Section 9 N135°E
SDR
Section 10 N135°E

Figure 5A

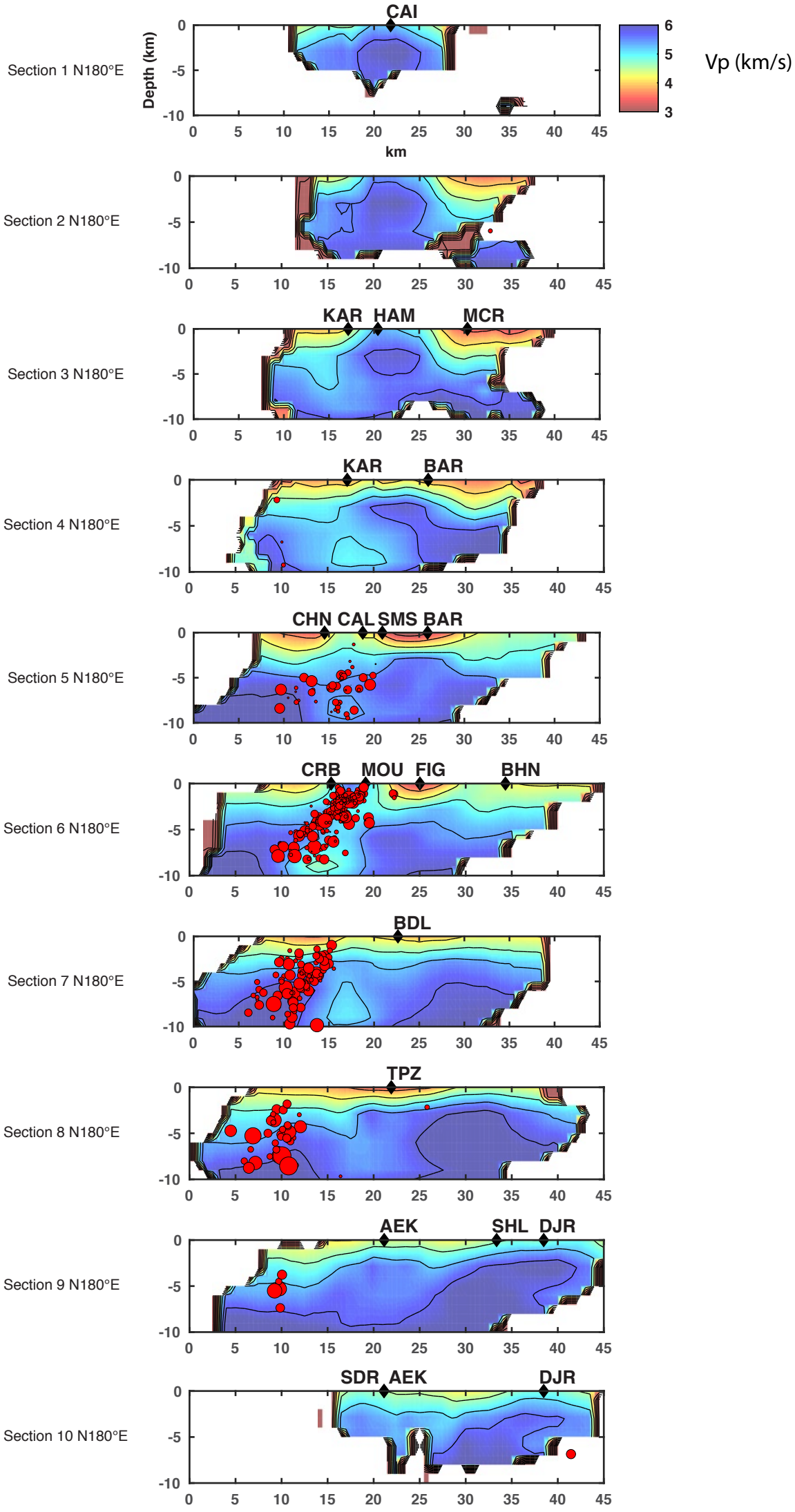
Section 1 N180°E
Section 2 N180°E
Section 3 N180°E
Section 4 N180°E
Section 5 N180°E
Section 6 N180°E
Section 7 N180°E
Section 8 N180°E
Section 9 N180°E
Section 10 N180°E
Depth (km)
km
Vp (km/s)
CAI
KAR HAM MCR
KAR BAR
CHN CAL SMS BAR
CRB MOU FIG BHN
BDL
TPZ
AEK SHL DJR
SDR AEK DJR

Figure 5B

Appendix

A1. WAM grids

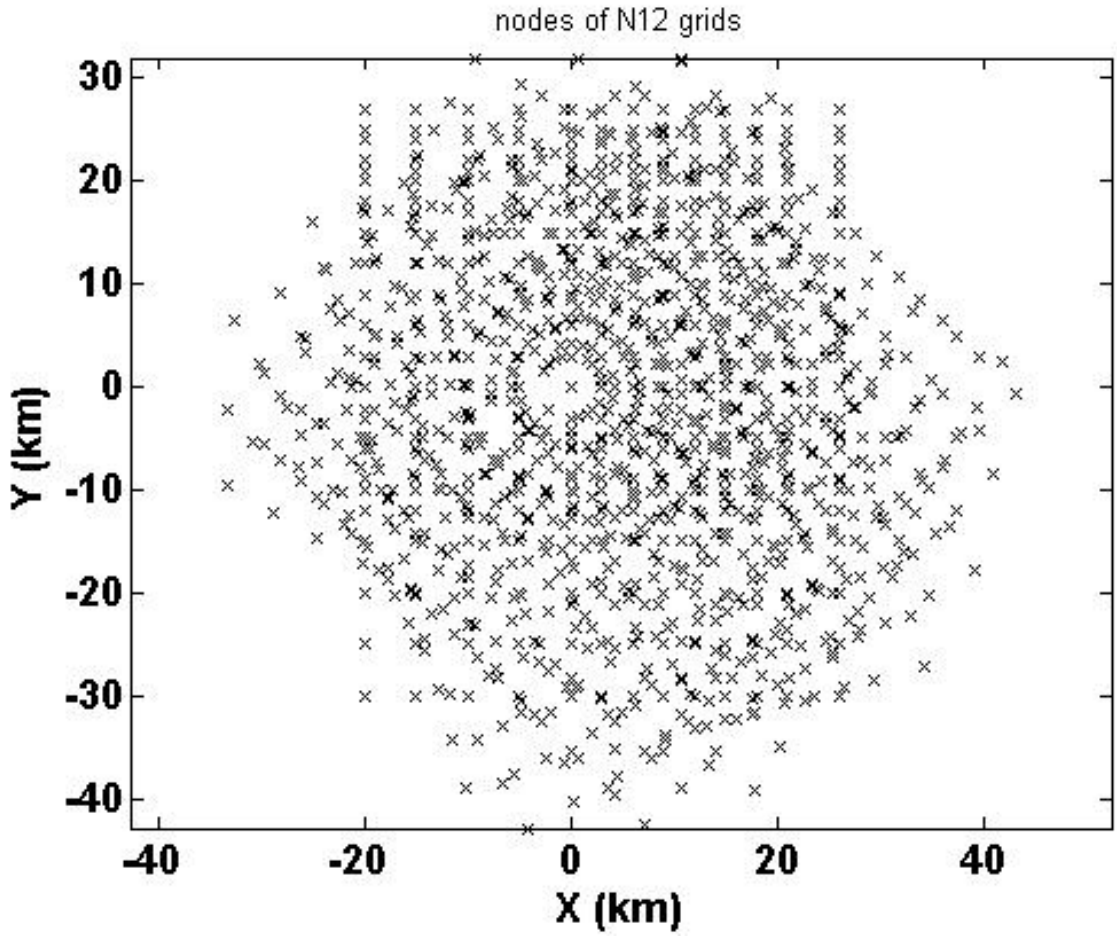

A2. Resolution of the velocity model

The figures show the Weighted Standard Deviation (WSTD) calculated directly from the velocity distribution from the previous 12 inversions, selected to build a final WAMs model. The latter allows to evaluate the stability and reliability of the inversion (Calo et al., 2013).

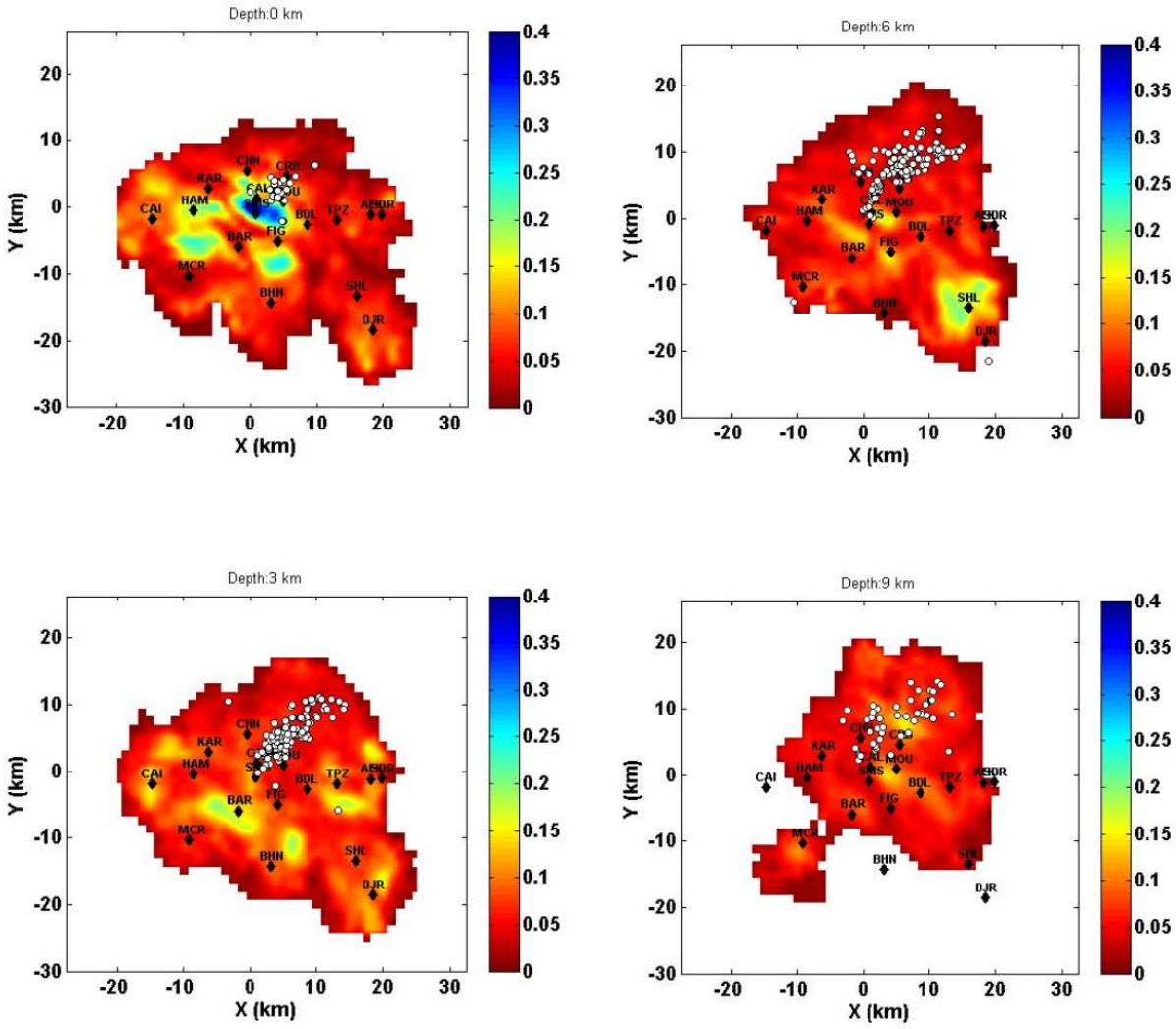

Table 1 Characteristics of major instrumental earthquakes of northern Algeria

#	Locality	date	longitude	latitude	depth	str1	dip1	rake1	str2	dip2	rake2	Mw	Mb	Ms	Reference
1	Orleansville	09.09.54	1.566	36.285	-	253	61	104	46	32	76			6.5	Espinoza & Lopez–Anoyo (1984)
2	Orleansville	10.09.54	1.241	36.617	-	44	90	-8	134	82	172			6.0	Dewey (1990)
3	El Asnam	10.10.80	1.36	36.25	14	225	54	83	57	36	80	7.1	6.5	7.3	Global CMT; Deschamps et al. (1982)
4	El Asnam	08.11.80	1.37	36.18	-	230	52	90					5.3		Ouyed et al 1981
5	Tenes	15.01.81	1.65	36.33	14.5	181	53	29	72	67	139	5.0		4.6	Global CMT/ISC
6	Oued Djar	31.10.88	2.73	36.35	-	103	55	167	201	79	36			5.4	Global CMT/ISC
7	Chenoua	29.10.89	2.43	36.62	10	246	56	86	71	34	94	5.9	5.8	6.0	Bounif et al. (2003)
8a	Tipaza	09.02.90	2.42	36.73	10	49	18	95	225	72	88		5.0	4.7	CSEM/CMT
8	Tipaza	09.02.90	2.48	36.78	15	49	18	95	225	72	88		5.0	4.7	Global CMT/ISC
9	Alger	04.09.96	2.81	36.9	-	11	76	-4	102	86	-166	5.5	5.3	5.3	Global CMT/CRAAG
10	Zemmouri	21.05.03	3.65	36.85	10	57	44	71	262	49	107	6.8		6.9	Global CMT/CRAAG
11	Zemmouri	27.05.03	3.79	36.94	15	70	31	92	248	59	89	5.7		5.5	Global CMT
12	Zemmouri	29.05.03	3.55	36.84	15	14	59	5	282	86	149	5.1		4.6	Global CMT